Quasi Steady State Effect of Micro Vibration from Two Space Vehicles on Mixture During Thermodiffusion Experiment

A.H. Ahadi[1] and M.Z. Saghir[1]

Abstract: The numerical simulations of a thermodiffusion experiment in atmospheric pressure binary mixtures of water and isopropanol subject to micro-vibrations at reduced gravity are presented. The vibrations are induced on board ISS and FOTON-M3 due to many different reasons like crew activity, spacecraft docking or operating other experiments, etc. The effects of micro-gravity vibration were investigated in detail on all of the mixture properties. The influences of different cavity sizes as well as different signs of Soret coefficients in the solvent were considered. In this paper, the thermodiffusion experiment was subjected to two different g-jitter vibrations on board ISS and FOTON-M3 as a cavity with a lateral thermal gradient, filled with a mixture of water and isopropanol, is numerically simulated. The full steady-state Navier-Stokes equations, as well as the energy, mass transport and continuity equations were solved numerically using the finite element method. It must be noted that two different methods to present micro gravity vibrational acceleration on ISS and FOTON-M3 were performed and programmed in MATLAB to find proper value of acceleration at any step time. All physical properties including density, mass diffusion and thermodiffusion coefficients were assumed variable as function of temperature and concentration using PC-SAFT equation of state. Assuming all physical properties to be variable made the results more practical in comparison with the constant model, particularly in the ISS cases. The separation behavior of isopropanol and water in terms of the concentration profiles as well as the thermodiffusion coefficients was in agreement with the experimental trends with a small discrepancy for FOTON cases; however, the ISS results show a strong single convection cell that disturbed the pure diffusion process.

Keywords: Thermodiffusion, Micro-gravity, CFD simulation, Binary mixture.

---

[1] Mechanical Engineering Department, Ryerson University, Toronto, Ontario, Canada M5B 2K3

1   Introduction

Thermodiffusion causes to the Soret effect, the chemical separation that is obtained by the thermal gradient in non-reacting mixtures, and is quantified by the Soret coefficients when there is no convection. The thermal diffusion phenomenon plays a vital role in the investigations of hydrodynamic stability in fluid mixture, movement of mineral, mass transport modeling in living matters and the compositional variation in hydrocarbon reservoirs (Duhr & Braun, 2011). Thermodiffusion is the diffusive coupling between heat transport and mass transport. By knowing the isothermal diffusion coefficients, thermodiffusion is determined by the corresponding Soret coefficients, the experimental quantities that relate the solute gradient to the thermal gradient in a closed system without convection or reaction and at steady state.

The Soret coefficients are known to be difficult to measure on ground conditions because of technical constraints in the control of spurious thermal and liquid convection and convective instabilities. Consequently, materials science, combustion science, low temperature microgravity physics, fluid physics, biotechnology and life sciences experiments are performed on the different lab orbiters in the space vehicles such as International Space Station or FOTON satellites, to take benefit from the reduced gravity environment. The residual acceleration environment of an orbiting spacecraft in a low earth orbit is a very complex observable fact. Many reasons, such as experiment operation, life-support systems, equipment operation, aerodynamic drag, gravity gradient, crew activities, and rotational effects as well as the vehicle structural resonance frequencies contribute to form the overall reduced gravity environment. Weightlessness is an ideal condition which cannot be assessed in practice as a result of the various sources of acceleration present in an orbiting spacecraft. Consequently, experiments can be affected by the residual acceleration due to their relation to acceleration magnitude, orientation and duration, frequency (Monti, Savino and Lappa, 2001; Srinivasan and Saghir, 2011). Hence, experimenters must know what the environment was when their experiments were executed in order to analyze and correctly interpret the consequence of their experimental data (Rogers, Hrovat, & McPherson, 2002). There are many publications in this field to measure the effect of g-jitter acceleration on thermodiffusion experiments. The thermal simulation of thermodiffusion in ternary hydrocarbon mixtures at high pressure was investigated by Srinivasan, Dejmeck, & Saghir (2010). It was found that the sign of the thermal diffusion coefficient for a given component in a mixture of more than two components cannot be related to the segregation of that component to the cold or hot wall. Thus, an approach to determine the mass and thermodiffusion coefficients is necessary for the governing equations. They used the special formulation by Shukla & Firoozabadi (1998) for the net heat of

transport in molar average velocity frame. Their thermodiffusion model has been coupled with the PR EOS[1] and has been validated against the experimental result (Platten, 2003). The author showed that the model performed well only for certain compositions. The influence of vertical high-frequency and small-amplitude vibrations on the separation of a binary mixture saturating a shallow horizontal porous layer heated from below has been studied Elhajjar, Mojtabi, Catherine, & Mojtab (2009).

Tai & Char (2010) surveyed the effects of thermodiffusion on heat and mass transfer by free convection flow. A review of experimental approaches to study thermodiffusion was done by Srinivasan & Saghir (2010). The results of this study are vital because it shows the significant role of vibration on the diffusion process. It can be found that performing microgravity experiments causes significant reduction in the convection issues discussed earlier and the results can serve as benchmark values if the microgravity experiments are successful; however, costs of these experiments are very high. Parsa, Srinivasan, & Saghir (2010) investigated thermo-solutal-diffusion in high pressure liquid mixtures in the presence of micro gravity vibrations. The results indicate a formation of a single convective cell in all the mixtures due to a steady static micro-gravity in both directions. It shows a stronger velocity component orthogonal to the direction of the temperature gradient. The separation behavior mixture in terms of the concentration profiles and the thermodiffusion coefficients matched with the experimental trends. They also predicted the change of the sign of thermodiffusion correctly. They used acceleration data that were obtained from the satellite by the onboard accelerometer (DIMAC[2]) for the source of vibration that affected the experiment. Their simulations and the experiment were made in rectangular cavity with same dimensions, so the actual micro-gravity environment was taken into account. Their results were in agreement with Yan, Jules, & Saghir (2008), who found that with an increase in the molecular weight of the second component of the mixture, the thermal diffusion coefficient values decreased. They explained the negative value of thermal diffusion coefficient as a result from a fact that in all mixtures methane tends to separate towards the hot side. They saw in their plots, near the walls, the velocity in the y-direction was two orders of magnitude larger than the velocity in the x-direction, which was in agreement with the pervious study by Chacha & Saghir (2005). Their conclusions were carried out based on the concentration profiles as well as the sign of the thermodiffusion coefficients of the two species. They concluded that FOTON missions provide a suitable platform to conduct the investigations of purely diffusive processes with minimal hindrance. Parsa & Saghir

---

[1] Peng Robinson Equation of State
[2] direct measurement micro-accelerometer

(2011) studied the Double-diffusive thermal convection with the Soret effect under different vibration condition when the steady gravity was assumed to be zero. This research was unique because all physical properties including density, mass diffusion and thermodiffusion coefficients were assumed to be functions of temperature and concentration using PC-SAFT[3] equation of state. The system was subjected to the three different levels of Rayleigh vibrations by using different frequencies, amplitudes and temperature gradients. The results show that using variable properties from PC-SAFT make the outcomes more reasonable in comparison with the model with constant properties. It is observed that a strong mixing was found in cases with high Rayleigh vibrations.

This paper is arranged as follows: Section 1 is an introduction; Section 2 describes the physical problem and governing equations as well as the two-dimensional numerical CFD simulation; Section 3 presents scenarios to calculate the g-jitter vibration on board ISS and FOTON-M3. Section 4 contains the result and discussion, a comparison between the ISS and FOTON mission to provide the thermodiffusion experiment board. Finally, section 5 is the conclusion.

2   Problem description and solution strategy

As shown in Fig. 1, the two-dimensional heat and mass transfer with Soret effect is considered for cavity sizes such as 10×10, 5×10, $10 \times 5\,mm^2$. Two vertical walls are at constant temperature, $T_h = 303K$ and $T_c = 293K$, yielding a temperature difference of 10 K. All other walls are assumed thermally insulated. An initially homogenous liquid mixture of water isopropanol is considered which water represents 90% mass fraction of the mixtures. However, in one case because of our interest in positive Soret and studding its effect, water content was 50% of the cavity. Under the applied temperature gradient, the two components of the mixture have a tendency to separate from each other due to the Soret effect.

2.1   *Governing equations*

The problem of double diffusion convection is governed by the mass conservation, species conservation and energy and momentum equations. Both molecular and thermal diffusion coefficients are assumed to be variable in the simulation based on by Shukla & Firoozabadi (1998). The governing equations for a binary mixture and 2D Cartesian system take the form:

$$\frac{\partial \rho}{\partial t} + \frac{\partial (\rho u)}{\partial x} + \frac{\partial (\rho v)}{\partial y} = 0 \tag{1}$$

---

[3] Perturbed-Chain Statistical Associating Fluid Theory
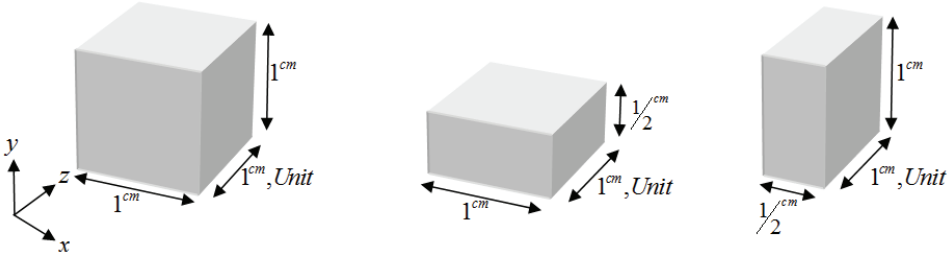
Figure 1: Three different considered cavities

$$\frac{\partial}{\partial t}(\rho c) + \frac{\partial}{\partial x}(\rho u c) + \frac{\partial}{\partial y}(\rho v c) =$$
$$\frac{\partial}{\partial x}\left[\rho\left(D_M\frac{\partial c}{\partial x} + D_T\frac{\partial T}{\partial x}\right)\right] + \frac{\partial}{\partial y}\left[\rho\left(D_M\frac{\partial c}{\partial y} + D_T\frac{\partial T}{\partial y}\right)\right] \quad (2)$$

$$\frac{\partial}{\partial t}(\rho T) + \frac{\partial}{\partial x}(\rho u T) + \frac{\partial}{\partial y}(\rho v T) = \frac{\partial}{\partial x}\left[\frac{k}{c_p}\left(\frac{\partial T}{\partial x}\right)\right] + \frac{\partial}{\partial y}\left[\frac{k}{c_p}\left(\frac{\partial T}{\partial y}\right)\right] \quad (3)$$

$$\frac{\partial}{\partial t}(\rho u) + \frac{\partial}{\partial x}(\rho u u) + \frac{\partial}{\partial y}(\rho v u) = -\frac{\partial p}{\partial x} + \frac{\partial}{\partial x}\left[\mu\left(\frac{\partial u}{\partial x}\right)\right] + \frac{\partial}{\partial y}\left[\mu\left(\frac{\partial u}{\partial y}\right)\right] + \rho g_x$$
$$(4)$$

$$\frac{\partial}{\partial t}(\rho v) + \frac{\partial}{\partial x}(\rho u v) + \frac{\partial}{\partial y}(\rho v v) =$$
$$-\frac{\partial p}{\partial y} + \frac{\partial}{\partial x}\left[\mu\left(\frac{\partial v}{\partial x}\right)\right] + \frac{\partial}{\partial y}\left[\mu\left(\frac{\partial v}{\partial y}\right)\right] + \rho g_y \quad (5)$$

where T is the temperature; ρ is the density; c is the mass concentration of the carrier which is water in this experiment; p is the pressure; u and v are the velocity components along the x and y-directions respectively; k is the thermal conductivity; μ is the kinematic viscosity; c_p is the specific heat and D_M is the molecular diffusion coefficient; D_T is the thermal diffusion coefficient. Equations 1 to 5 define the conservation of mass, single species, energy, momentum along the x and y-directions respectively. As governing equations show, density and viscosity in mixture are variable. They were assumed to be functions of concentration at each

point; this assumption makes this work unique and stronger than other works which studied micro-gravity effects on thermodiffusion experiment. See Eq. 6, and 7 which show viscosity and density equation as a function of concentration.

$$\mu = c_1\mu_1 + c_2\mu_2 \tag{6}$$

$$\rho = \left(\frac{c_1}{\rho_1} + \frac{c_2}{\rho_2}\right)^{-1} \tag{7}$$

where $\rho_1, \rho_2, c_1, c_2, \mu_1, \mu_2$ are density, mass fraction and viscosity of the pure components (water/isopropanol) respectively.

2.2   PC-SAFT Equation of State

It should be mentioned that density is a function of temperature as well as mass fraction through the PC-SAFT equation of state (Joachim & Gabriele, 2001). It is used in this study for association mixture because in PC-SAFT equations an association term is considered, in order to account for intermolecular force. By modeling these forces more accurately, the chance of having a better prediction of the conditions when associating compounds will exist in a gas or liquid phase will be increased. According to this model; molecules are determined by three pure component parameters. The first parameter is segment diameter. Second of all, segment number and the last one, is attraction parameter which also presents in the original SAFT equation of state. Thus, the dispersive forces are considered for applying a perturbation theory of the second order, using an expression for the radial pair distribution function of a hard-chain reference fluid (Joachim & Gabriele, 2001).

2.3   Boundary and initial conditions

The assumptions for boundary conditions for the velocity, temperature and diffusion flux are as follow first of all, the walls are rigid, so there in no flow; thus, no slip boundary condition must be applied. Moreover, the two vertical walls of the cavity are kept at constant hot and cold temperature. It should be noted that all other walls are adiabatic. At the end, there is no reaction inside the cavity and no mass flux through the cavity walls. For initial condition, the velocity is equal to zero, the concentrations of each component is set to be uniform at the domain and equal to the initial concentrations at the beginning of the simulation. The pressure of the mixture in cavities is assumed to be atmospheric pressure at sea level. The other initial values of properties between hot and cold wall such as temperature and density are calculated based on average temperature between hot and cold wall.

$$at\ x = 0,\ \ x = L \tag{8}$$

$$u = 0, \quad v = 0 \tag{9}$$

$$T|_{x=0} = T_h, \ T|_{x=L} = T_c \tag{10}$$

$$J_x = D_M \frac{\partial c}{\partial x} + D_T \frac{\partial T}{\partial x} = 0 \tag{11}$$

at $y = 0, \quad y = H$

$$u = 0, \quad v = 0 \tag{12}$$

$$\frac{\partial T}{\partial y} = 0 \tag{13}$$

$$J_y = D_M \frac{\partial c}{\partial y} + D_T \frac{\partial T}{\partial y} = 0 \tag{14}$$

The above equations show the mathematic form of boundary conditions, where J_i is the flux in the ith direction. x and y represent the position in two perpendicular directions, L is the length of the cavity, H is height of the cavity; L and H are defined based on cavity dimensions.

2.4   The numerical method

Numerical discretization of the governing equations under the influence of g-jitter accelerations are carried out using a finite volume method. So, the discretization is carried out with respect to the primary variables, pressure, temperature and composition. The previous governing equations were obtained for each grid block using a central finite-difference scheme in space on a Cartesian grid and a first-order finite-difference approximation for the derivative in the accumulations term, in time. The physical properties used in this study are given in Table 1. Eq. 1 to Eq. 7, include seven unknowns, (u, v, w, ρ, p, T, c) to be solved for each mesh point in the domain. To solve the governing equations, the SIMPLE[4] algorithm (Patankar, 1980) is executed.

The basic idea behind the SIMPLE method is to guess the pressure of the system, and find properties of the fluid as result of this guess, when making correction to this guess based on previous result and continuing the next iteration. For instance, $p*$ is the guessed pressure and p' is a parameter for improving the guessed pressure such that the resulting starred velocity field will progressively get closer to satisfying the continuity equation. Thus, the correct pressure p, may be defined according following equation;

$$p = p* + p' \tag{15}$$

---

[4] Short term of Semi-Implicit Method

Table 1: Fluid Properties

	Water	Isopropanol
viscosity$[g/(m.s)]$	0.923	2.0553
Molar volume at$[cm^3/mol]$	18.81	82.97
Critical Temperature $[k]$	647.29	508.30
Critical Pressure $[MPa]$	22.090	4.762
Molecular weight $[g/mol]$	18.015	60.096
Density$[kg/m^3]$	984	905
Thermal Conductivity $[w/m.K]$	0.5220	0.2866

After this correction the velocity components responding to this change in pressure should be found. The corresponding velocity corrections u', v' can be introduced in a similar manner,

$$u = u* + u' \quad v = v* + v' \tag{16}$$

Then, the new correction velocity is calculated from their starred values using the velocity-correction formulas. After that, discretization equation for other properties like temperature and concentration is solved. For the next iteration, treat the corrected pressure $p$as a new guessed pressure$p*$,when to return to first step of iteration. It is necessary to repeat the whole procedure until a converged solution is obtained. In each step of this iteration process, the average relative error of u, v, p, T, ρ and concentration are computed as F_u, F_v, F_p, F_T, F_ρ and F_{c_i}, respectively, where F is defined as follow;

$$F_\varphi = \frac{1}{n \times m} \sum_{i=1}^{m} \sum_{j=1}^{n} \left| \frac{\varphi_{i,j}^{t,s+1} - \varphi_{i,j}^{t,s}}{\varphi_{i,j}^{t,s+1}} \right| \tag{17}$$

In the above equation, t is the time step, s is the iteration number and (i,j) represent the cell on the grid. A convergence is achieved if the results of function F for all the unknowns are below 1×10^{-6} in two continue successive iterations. The maximum number of iterations within each loop is five thousand, after which if convergence has not been reached, the time step increment is divided by a factor of two and the loop begin again.

2.5 *Mesh Sensitivity Analysis and Time Step Control*

Performing a mesh sensitivity analysis is an integral part of producing accurate, time-efficient and cost-effective results. For this study, we used the same mesh as

used by Parsa & Saghir (2011). He used a mesh of 17 elements in the x-axis by 17 elements in the y-axis for the two-dimensional laterally heating conditions for a cavity of one centimeter length and height. Thus for other cases which are smaller than first cavity, cells of the same diameter of smaller has been used.

In order to obtain sufficient accuracy, while maintaining optimal processing time, the value of the incremental time step must be chosen carefully. One of the major goals of this study is to find the best time step for our problem so that the accuracy and computational time remain optimal. The initial time step is set to 0.02 s.

3   Accelerometer Data Analysis

The goal of the detailed analysis is to use all available vibration raw data in our simulation model. The reasons that we need this analysis are, first the time step of the raw data; thus, these methods are required to change the raw data to acceleration with our interested step time. Secondly, in the raw vibration data, there is no reference; consequently, it is necessary to demean the raw data over special period of time.

3.1   ISS acceleration

SAMS[5] determines accelerations caused by vehicle, crew and equipment disturbances. SAMS measures the vibratory, transient accelerations, which take place in the frequency range of 0.01 to 300 Hz. For Increment-2, there are five SAMS sensors along with experiments located in the ISS. Mean-square acceleration is the average of the square of the acceleration over time. If the acceleration is a pure sinusoid with zero mean value, e.g., a steady-state vibration, the RMS acceleration would be 0.707 times the peak value of the sinusoidal acceleration. The following definitions provide clarity and guidance for the understanding of the terms. The equation of RMS was provided in the following;

$$X^{RMS} = \sqrt{\frac{\sum_{i=1}^{n} x_i^2}{n}} \tag{18}$$

It should be note that Eq. 17 is just used for a discrete distribution. The equations below show the RMS method to calculate the values of acceleration during the specific time step (0.02 s) to apply to the CFD simulation code,

$$\vec{g} = g_x^{RMS}.\vec{i} + g_y^{RMS}.\vec{j} \tag{19}$$

---

[5] Space Acceleration Measurement System

where

$$g_x^{RMS} = \sqrt{\frac{\sum_{i=1}^{n} (g_{x,i}^{ISS} - \bar{g}_{x,i}^{ISS})^2}{n}} \qquad (20)$$

$$g_y^{RMS} = \sqrt{\frac{\sum_{i=1}^{n} (g_{y,i}^{ISS} - \bar{g}_{y,i}^{ISS})^2}{n}} \qquad (21)$$

$$\bar{g}_{y,i}^{ISS} = \frac{\sum_{i=1}^{m} g_{y,i}^{ISS}}{m} \qquad (22)$$

In the above equations, g_x^{ISS} and g_y^{ISS} are the raw acceleration in the x and y-direction respectively, recorded by the SAMS accelerometer onboard the ISS. n is number of data during the special time step or interval. $\bar{g}_{y,i}^{ISS}$ is the average acceleration in a ten-minute interval; m is the number of raw acceleration data in a PAD file or the number of recorded data in each ten minutes. Typical RMS accelerations in a 45 second interval that were applied in the simulations in this study are shown in Fig. 2.
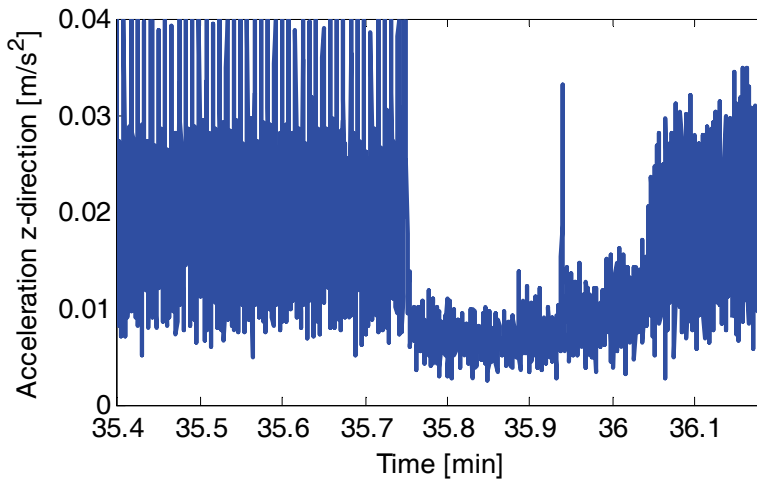
Figure 2: Vibration along y-direction on board ISS

3.2   FOTON-M3 acceleration

For both the FOTON and ISS acceleration versus time, is archived; however, the time step for FOTON was about half a minute while this parameter for ISS was

about 0.02 s, and based on this, it is necessary to interpolate between each two steps. There are some previous similar attempts to apply the acceleration by interpolating between two points (Srinivasan, Dejmeck, & Saghir, 2010). They used linear interpolation between each two steps to find the acceleration that must be applied in the system between two continues step times. In Fig. 3, the solid lined shows their interpolation and dashed line showed higher order of interpolation by curve. The dashed line shows the vibration which is closer to reality.
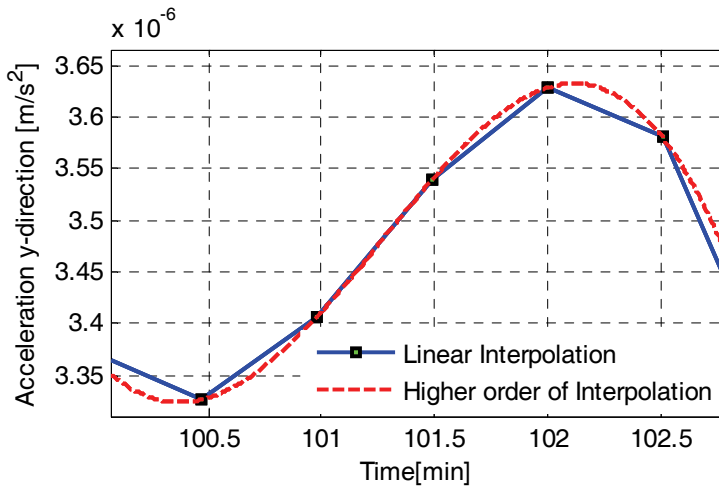
Figure 3: Acceleration along y-direction on board FOTON-M3

Interpolation between all points as a special polynomial function is almost impossible. To solve this issue we chose several consecutive points and fit the curve to them. When we repeat it for next several points. However, the same problem occurs in this method between each level of interpolation from one step to another. To remove this issue, in each level of the procedure, the MATLAB code reads one point before the first point and one after the last point of that specific level and fits the curve, which is two orders larger than the total number of the points on that level of procedure.

4   Results and Discussion

CFD simulations were performed for all the nine cases. In this simulation four of them were investigated onboard FOTON-M3 and four on board ISS. In addition to have clear comparison with the pure diffusion process, the ninth case was assumed to be an ideal case without any vibration and gravity, See Table. 2.

It was observed that the average acceleration in the x and y-directions on board ISS was about $20 mm/s^2$; however, this quantity for FOTON-M3 was less than $18 \mu m/s^2$. Although both of these values are too small to consider them as acceleration, in the thermodiffusion experiments they have effects. Another important point is the ratio of magnitude of acceleration between ISS and FOTON.

Table 2: Characteristics of the each binary Cases

Case	Plat Form	Isopropanol Mass Fraction	Cavity Size	Mesh Resolution
1	ISS	0.10	$1 \times 1 \left[cm^2\right]$	17×17
2	FOTON-M3	0.10	$1 \times 1 \left[cm^2\right]$	17×17
3	ISS	0.50	$1 \times 1 \left[cm^2\right]$	17×17
4	FOTON-M3	0.50	$1 \times 1 \left[cm^2\right]$	17×17
5	ISS	0.10	$1 \times 0.5 \left[cm^2\right]$	32×17
6	FOTON-M3	0.10	$1 \times 0.5 \left[cm^2\right]$	32×17
7	ISS	0.10	$0.5 \times 1 \left[cm^2\right]$	17×32
8	FOTON-M3	0.10	$0.5 \times 1 \left[cm^2\right]$	17×32
9	Ideal	0.10	$0.5 \times 1 \left[cm^2\right]$	10×30

The ISS vibration is one thousand times stronger than that of FOTON. All simulations were performed for about two hours until a quasi-steady state was reached, this duration was used based on previous investigations performed by Saghir and his team (Parsa, Srinivasan, & Saghir, 2010) (Parsa & Saghir, 2011)(Srinivasan, Dejmek, & Saghir, 2010). It was found that the separation in a mixture is dictated by the probability of an interaction between two molecules of different components. The probability of these events is dictated by the activation energy, size of the molecules and the mole fractions of the individual components in the mixture, for more detail about this theory see (Srinivasan & Saghir, 2009).

4.1   Spatial Analysis

All mixtures reached a quasi-steady state by about 8500 seconds. At this point, for all mixtures, almost a linear variation of the parameters, such as the fluid temperature and species concentration, was established from the hot wall to the cold wall for FOTON cases. A similar linear variation was observed at each horizontal level in the cavity. Due to the Soret effect, generally isopropanol separates towards the cold wall and water moves to the hot wall.

The strong mixing in the ISS cases is evident in the form of large velocities in the cavity along x-and y-directions at about 2.5 hours in Fig. 4 part (b). Fig. 4 part

(a) shows the mass fraction of isopropanol for FOTON, that means case 2 based on Table 2. Moreover part (b) shows this fraction for ISS, which is case 1 according to that table 2. As one can see in these figures, separation on FOTON-M3 occurred in a manner similar to the pure diffusion phenomena, while for ISS this phenomenon is not only visible, but also strong convection resulted from buoyancy forces that made a strong mixing in the cavity.

(a) FOTON-M3; Initial concentration c =0.1   (b) ISS; Initial concentration c= 0.1
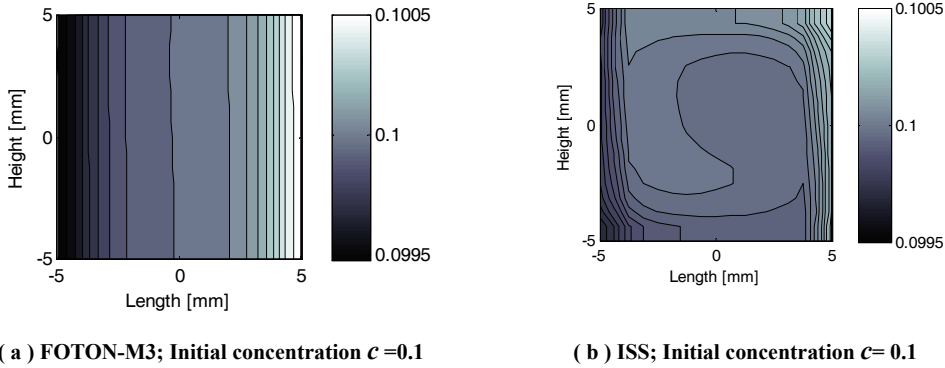
Figure 4: Isopropanol mass fraction distribution in cavity

(a) FOTON-M3   (b) ISS
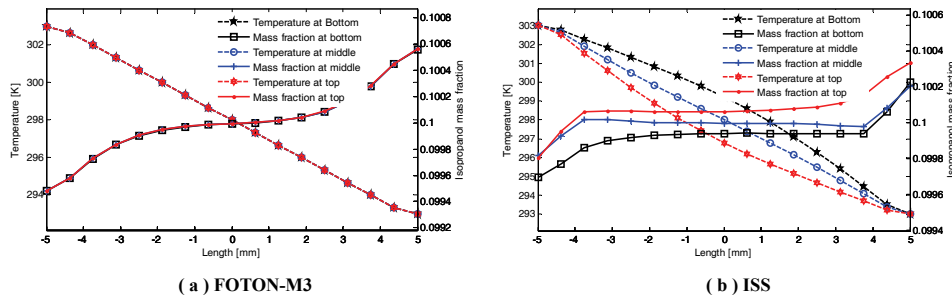
Figure 5: Temperature and Isopropanol mass fraction variation along x-direction

It is obvious that for the ISS cases at the top of the cavity near the cold wall, there is a maximum concentration of isopropanol and a minimum isopropanol mass fraction at the bottom near the hot wall; however, this observation is reversed for water mass fraction. Consequently, there is a variation of isopropanol mass fraction along the vertical lines in the cavity for the ISS case. In comparison, for FOTON-M3 the fractions of components near each wall remained the same. Moreover, it

(a) **FOTON-M3**   (b) **ISS**
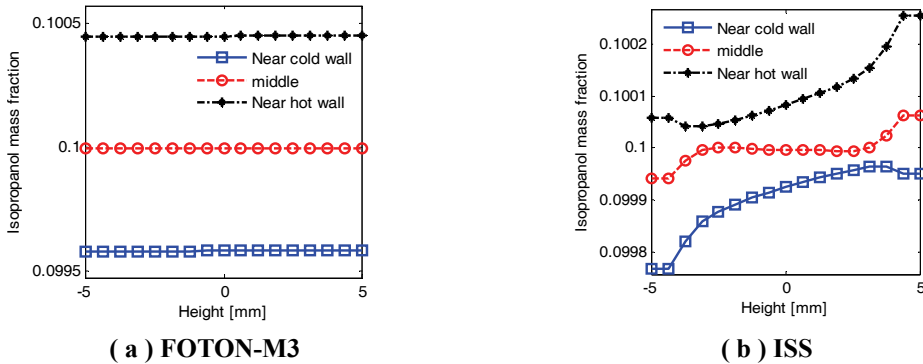
Figure 6: Isopropanol mass fraction variation along y-direction

must be added that for both cases the mass fraction of water near the hot wall is less than that near the cold wall while isopropanol were trapped near the hot wall. Fig. 5 shows the mass fraction of isopropanol, along three different horizontal lines at the bottom, middle and top of the cavity for cases 1 and 2. Despite a constant initial mass fraction of 0.1 in both cases, the separation in case 2 was more pronounced than in the ISS case as a result of a strong convection cell in ISS cases. All lines are overlapped on each other for FOTON, which proves that there was a smooth diffusion environment, while at the top of case one, a slightly higher mass fraction of isopropanol was observed. It should be added that although the mass fraction at the top of the cavity is higher than at the bottom, the separation along of these horizontal lines is the same. In other words, a small gradual shift of mass fraction in the direction perpendicular to the temperature gradient is observed.

Fig. 6 illustrates the mass fraction of isopropanol, along three vertical lines near the hot and cold wall as well as the middle of the cavity for cases 1 and 2. Again, despite a constant initial condition for both cases, the vertical separations are not similar to each other; in case 2, concentration along vertical lines remained constant, while this quantity has changed strongly in the ISS cases. Two opposite curvatures were observed for isopropanol mass fraction along the y-direction at the top and bottom of the cavity. We can claim that this behavior at the center of the cavity and the bottom half of it is affected by the hot wall and the top half is affected by the cold one.

4.2 *Velocity field and Stream function*

It is observed that at the quasi steady state a single convective cell was established as shown in Fig. 7 for both ISS and FOTON cases. This is due to a dominant

induced velocity in the cavity. Although, these single cells are similar to each other, to have better view of the strength of these convection cells, the magnitude of the fluid velocity is required.

(a) FOTON-M3

(b) ISS
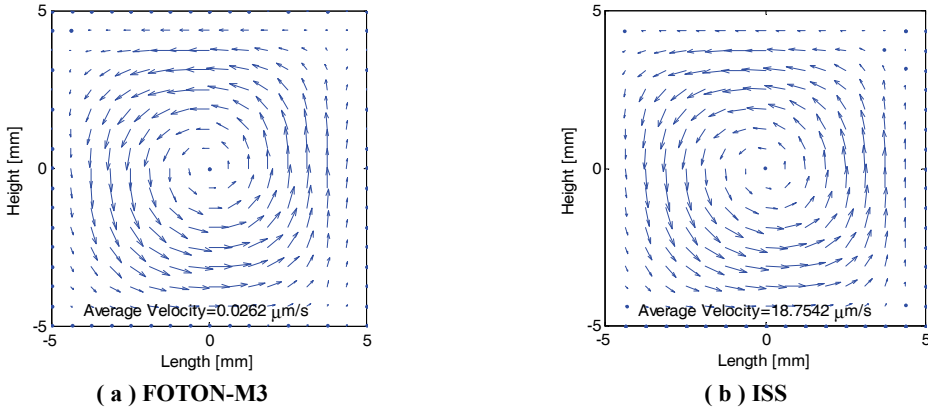
Figure 7: Velocity field in the domain at quasi-steady condition

(a) FOTON-M3

(b) ISS
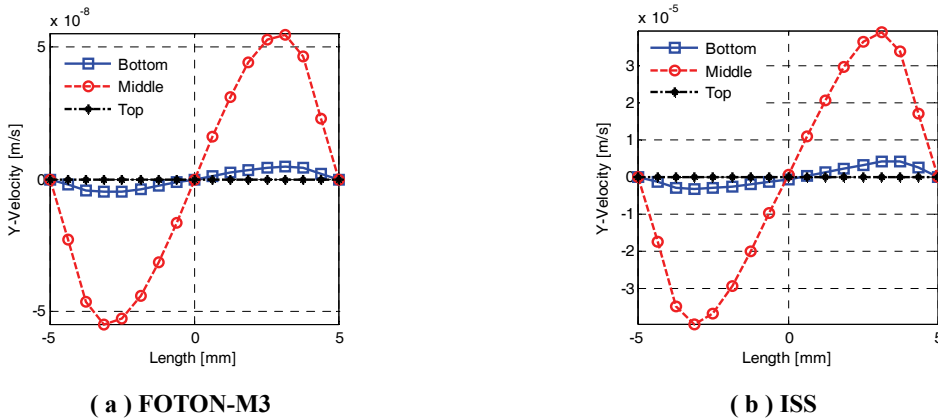
Figure 8: y-velocity variation along the x-direction

As mentioned , the average velocity to compare the strength of these cells is used. This means that for ISS cases the velocity is about 18 μm/s and for FOTON cases it is observe to be close to 0.02 μm/s. There is an interesting observation between vibration acceleration and this velocity which can be defined as follows. The logarithmic difference between vibration acceleration and average induced velocity was

(a) FOTON-M3   **(b)   ISS**
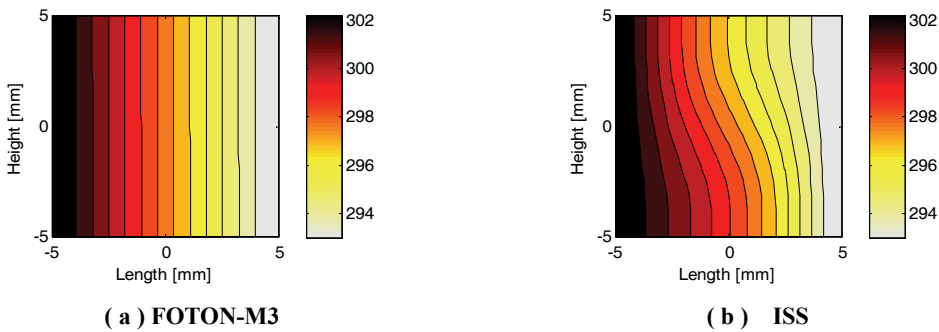
Figure 9: Temperature distribution in the domain [K]

similar for all cases even if we compare the results of the ISS to FOTON; this loga-
rithmic difference was calculated to be equal to 3 approximately. It should be noted
that to prove these relations further investigations is underway and we just claim
that such a relation may exist between velocity and acceleration; this relation would
be function of other characteristics of the vibrational acceleration like its frequency.
For the component of velocity along the y-direction, the line at the center has the
maximum magnitude, see Fig. 8. The y-velocity for both the ISS and FOTON-M3
behave completely like each other. The only difference is the order of the velocity
which occurs as result of different levels of vibrational acceleration these two on
the ISS and FOTON.

Temperature distribution   Fig. 9 shows the temperature contours in the cavity
for the quasi steady state condition for both the ISS and FOTON cases. From this
figure, it can be seen that for FOTON, the temperature contours are almost verti-
cally parallel. While temperature in the ISS case was affected by strong induced
convection as a result of vibration. Thus it can be concluded that, unlike the FO-
TON Temperature behavior which has similar variation for all horizontal lines, in
the cases of the ISS, as result of the strong convection cell, the temperature at the
top of the cavity experiences the a colder regime than at the bottom. Moreover, the
variation between the hot and cold walls is not linear except along the line at the
middle of the cavity. It should be noted that the maximum temperature variation
was observed for the vertical line at the center of the cavity for all ISS cases.

Diffusion coefficient   Fig. 10 shows molecular and thermodiffusion coefficients
variation along the length of the cavity. At least two important points can be con-
cluded from these figures. The first one is the importance of considering these
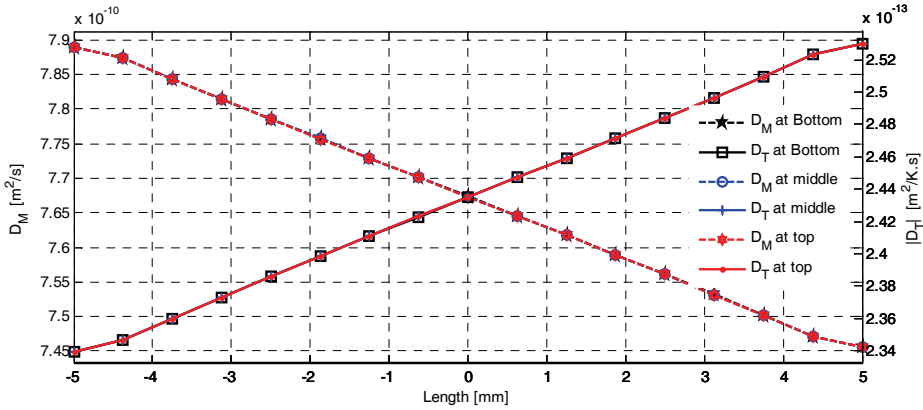
(a) FOTON-M3
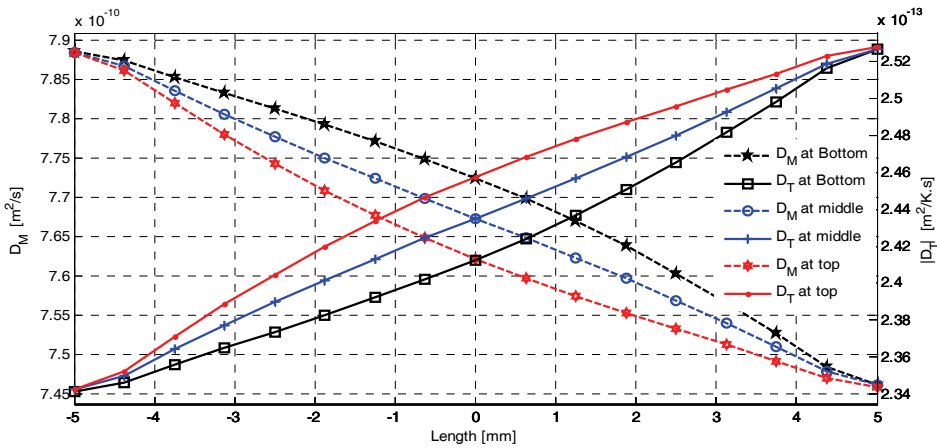
(b) ISS

Figure 10: Diffusion coefficients variation along x-direction

coefficients in the cavity to be variable, because a wide range of variation can be seen. As a result of a comparison between temperature variation and diffusion coefficients in Fig. 5 and Fig. 10, one can see a similar pattern for all of these properties. As expected the thermodiffusion coefficient is a function of temperature over the domain, while the similarity between temperature contour and molecular diffusion coefficient is a point that required more study to find out, whether the similarity occurs spontaneously or not. The variations of these coefficients are similar for both cases, while, like the other parameters, these coefficients very linearly

for FOTON-M3, but in the ISS case, two opposite curvatures were observed for horizontal for the horizontal lines at the top and the bottom of the cavity. Another important observation is the opposite behavior of magnitude of these coefficients along the cavity. In other words, the magnitude of the D_T increased but D_M decreased along the length of the cavity or from the hot to the cold wall. In addition, the horizontal line with the maximum value of thermodiffusion coefficients has the minimum molecular diffusion coefficient.

(a) $\rho[kg / m^3]$; **FOTON-M3**   (b) $\rho[kg / m^3]$; **ISS**
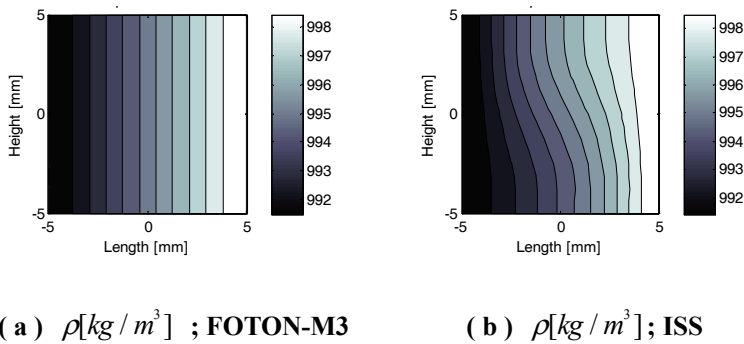
Figure 11: Density distribution in the domain

(a) $\mu[kg / (m.s)]$; **FOTON-M3**   (b) $\mu[kg / (m.s)]$; **ISS**
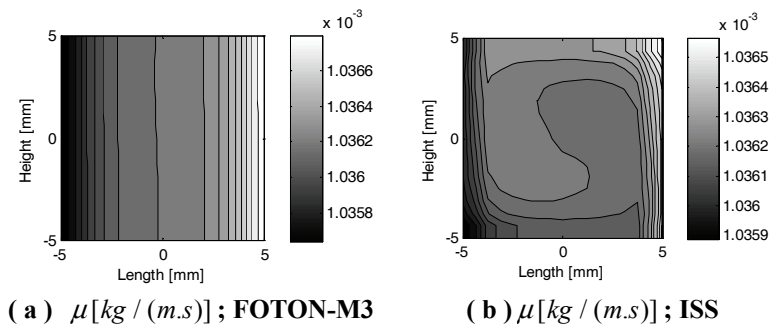
Figure 12: Viscosity distribution in the domain

Density and Viscosity   The last properties of the mixture which will be discussed are density and viscosity. As mentioned in section 2, the density of the mixture at each node was found by using the PC-SAFT equation of state, which shows a good performance for associating mixtures like water isopropanol. The values of the density over the cavity illustrate that this property was strongly dependent on

the temperature in this experiment and, because of the initial mass fraction of water in the mixture, the density values are mostly close to water density.

In most of the previous researches in this field, the viscosity was assumed to be constant, but in this study it was assumed to be variable by a special formulation which is explained in section two. Unlike density, viscosity is mostly a function of concentration and follows the same pattern as mass fraction of isopropanol in the mixture. It must be added, although this variation for density and viscosity are less than one percent, the importance of considering these properties to be variable could be understood from Fig. 11 and Fig. 12.

4.2.1   Cavity size effect

The size effect on convection in a square cavity and vertical and horizontal rectangle was numerically studied in this section. Zeng-Yuan, Zhi-Xin, & Xiao-Bing (2002) discussed the relative importance of three control forces of free convection, inertial-force, viscous-force and buoyancy-force as well as the variations of the three control forces with Rayleigh number. Their results explain that the effect of viscous force compared to the inertial force on the convection increasing with the diminishing size. In this study three different cavity sizes are considered, square cavity, one centimeter each side; rectangular cavity one centimeter by half and another rectangular cavity half centimeter by one.

Fig. 13 shows the concentration counter for different cavity size on board the ISS and FOTON. As in the last observation, the linear variation along the temperature gradient was seen for FOTON cases; however, the variation of these concentrations for the vertical rectangle is a bit greater than for the horizontal one. The same observation can be seen for ISS cases but the variation as a result of the strong convection cell is not linear. It was observed that by decreasing the length of the cavity, the temperature contour became more linear and more like the FOTON cases. In other words, again we can understand that the effect of thermal diffusion became more effective than the effect of convection when we compare the cavity with the same length and height with the horizontal cavity. Fig. 13 shows the isopropanol mass fraction along the temperature gradient at the middle of the cavity for FOTON and ISS respectively. It is clear that, pure diffusion in comparison with convection becomes more important and even dominant with the size reduction along the direction of temperature gradient. On the other hand, the concentration variation for cases with the same

height are similar to each other with very small difference as shown in Fig. 14. In conclusion, on this section we can claim that for the isopropanol mixture, the height of the cavity does not affect the results; however, by increasing the length of the cavity, the separation will become weaker and weaker.
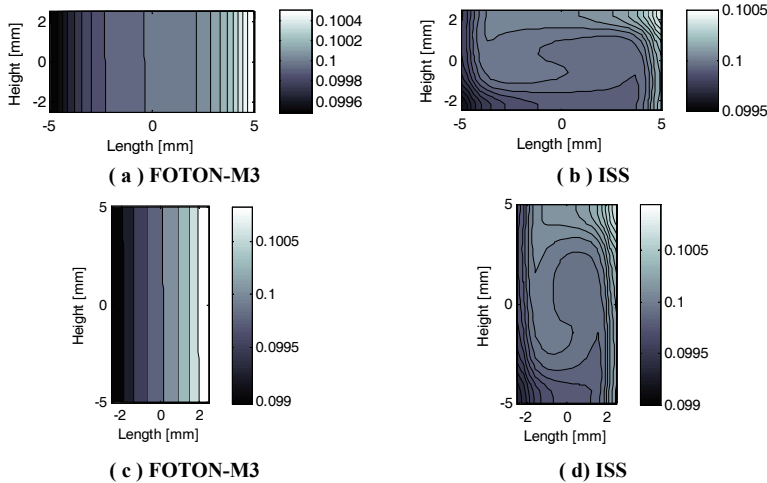
Figure 13: Isopropanol mass fraction distribution in the domain
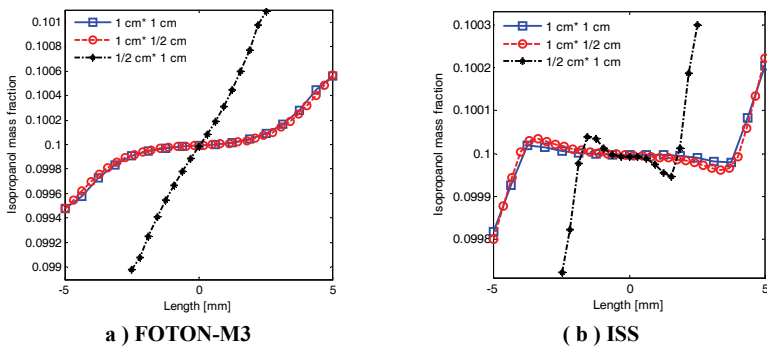
Figure 14: Isopropanol variation along x-direction respect to different cavity size

4.2.2 *Different initial concentrations*

In cases five to nine and mixtures one and two, the dominants of water decreases and that of isopropanol increases near the hot wall. In these mixtures, as a result of the high mass fraction of water, the negative Soret effect was observed during the thermodiffusion process. Likewise, in the mixtures three and four, due to the isopropanol high mass fraction is likely to dictate the thermodiffusion process. The weaker separation is attributed to the reduced molecular weight inequality that has been observed by Yan, Jules, & Saghir (2008). The different amount of separation is the other important observation made in this section, and shows this fact

that when there is positive Soret effect, the amount of separation was less than the case with negative Soret; see Fig. 15. To have clear understanding of the effect of positive Soret values, Fig. 16 was used; which part (a) shows the separation versus length of the cavity for negative Soret values, and part (b) shows this for negative Soret values. It is obvious that the concentration gradient magnitude for the positive Soret effect is less than the negative one. Because of different initial concentrations in these mixtures, it is impossible to compare them in the same scale of mass fraction. Consequently, we had to define a new term to refer to absolute concentration difference from, its initial value.

(a) **FOTON-M3; Initial concentration** c= 0.5   (b) **ISS; Initial concentration** c= 0.5
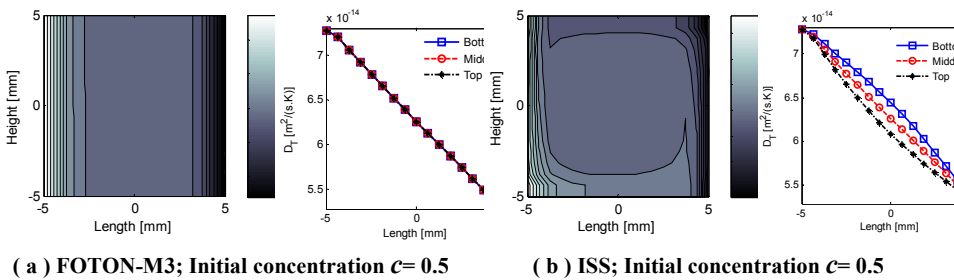
Figure 15: Isopropanol mass fraction and thermodiffusion coefficient respect to different initial concentration

(a) Initial concentration c= 0.1   (b) Initial concentration c= 0.5   (c) Spatial separation along the x-direction
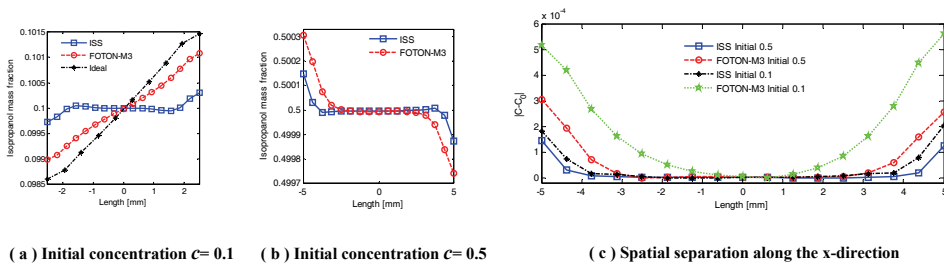
Figure 16: Isopropanol mass fraction and spatial separation for cases 1,2,3,4 and 9

Fig. 16 also shows that ISS cases have minimum separation but in a different direction of separation and with almost the same values for negative and positive Soret effects. However, for both FOTON cases, separation occurred more strongly than for ISS. Separation in the case with negative Soret effect has the biggest value.

This difference is explained as an unsteady condition for the cases with positive Soret. In Fig. 15, the contour illustrates mixing at the center of the cavity for both the FOTON and ISS cases. For all cases, the thermodiffusion coefficient increased from the hot wall to the cold one; however, as mentioned before for FOTON cases, as a result of pure diffusion, all lines coincide. The positive value of D_T indicates that in these mixtures water tends to separate towards the hot side. On the other hand, all other cases have negative thermodiffusion coefficients. This change in the sign of D_T shows the movement toward the cold or hot side.

4.2.3   Comparison between FOTON-M3 and Ideal case

Because of very weak vibration on board the unmanned satellite, we can see that it behaves mostly like the ideal case; however, the effect of the convection cell should be considered. In order to understand the contribution of such small induced velocity disturbances towards the thermodiffusion process, simulations were repeated by suppressing these external vibrations. In other words, the mixtures were simulated in an ideal zero-gravity environment. Interestingly, the results showed that, although the variations for FOTON were almost insignificant, they affected the final result of the experiments.

Fig. 16 part (a) shows isopropanol mass fraction along the x-direction of the cavity, which shows that, although the separation and diffusion in the FOTON case is much stronger than in the ISS case but is not a stronger as in the ideal case. In Table 3, three different approaches were used to define numerical parameter which shows this difference numerically. The first approach was to find the nodes with the maximum and minimum mass fraction and to calculate their difference. The second at steady condition was to find the average concentration at half of the cavity near the hot wall; the last approach was to find the concentration gradient per unit at the center of the cavity along a horizontal line. One can see that, for all cases, the value of the separation parameter for FOTON in greater than corresponding value for the ISS case, see Table. 3.

As mentioned before, the cases which have higher length assign lower value to separation. However, changing the height of the cavity does not affect the result very much. The minus sign for cases three and four means a positive Soret coefficient and unsteady condition; thus, the amount of the separation in these two cases is less than in any of the others. The last major difference between FOTON and zero gravity or the Ideal case was the pattern of their stream lines. As shown in Fig. 17, there was one strong convection cell in the FOTON case; however, for the Ideal case, we observed that there were four weaker convection cells in the cavity. We can claim that this difference occurs as a result of g-jitter vibration. The following formula is used to calculate the percentage error for FOTON and ISS in comparison

Table 3: Numerical result to compare different cases

Case	Plat Form	Isopropanol Initial mass fraction	Maximum Concentration difference	Mean Mass Fraction at half of the cavity near the hot wall	Maximum Concentration gradient per unit length []
1	ISS	0.10	0.0005564	0.09996	0.038929
2	FOTON-M3	0.10	0.0010835	0.09980	0.108212
3	ISS	0.50	0.0003168	0.50002	-0.0273
4	FOTON-M3	0.50	0.0005655	0.50007	-0.0565
5	ISS	0.10	0.0008027	0.09996	0.0424
6	FOTON-M3	0.10	0.0010855	0.09983	0.1085
7	ISS	0.10	0.0012748	0.09991	0.1157
8	FOTON-M3	0.10	0.0021122	0.09944	0.4219
9	Ideal	0.10	0.0028723	0.09915	0.5744

(a) **FOTON-M3**   (b) **Zero-gravity**
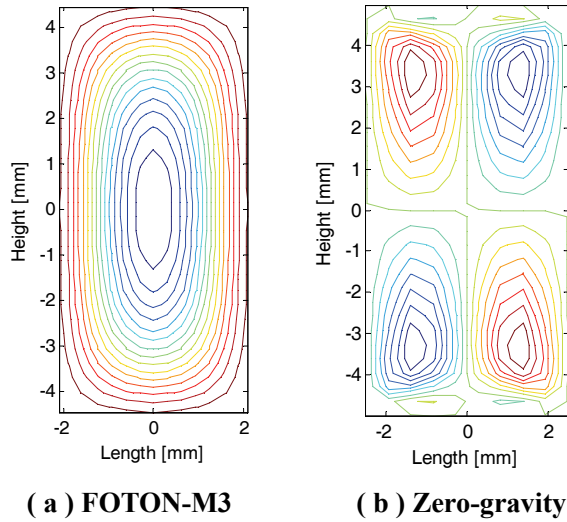
Figure 17: Cavity stream

with the zero-gravity condition.

$$E_\varphi = \left| \frac{\varphi_{Zero\ gravity} - \varphi_{micro\ gravity}}{\varphi_{Ideal\ Case}} \right| \times 100 \qquad (23)$$

where $\varphi_{Zero\ gravity}$ and $\varphi_{micro\ gravity}$ are the values of the parameter in a zero-gravity and micro-gravity environment, like FOTON or ISS, respectively. Table 4 shows these errors for ISS and FOTON-M3, if we assumed these to be zero-gravity environments.

Table 4: Percentage Errors

	ISS	FOTON
maximum Concentration difference	**55.6**	**26.4**
separated of Isopropanol at half of the cavity	**89.6**	**35.1**
maximum Concentration gradient per unit length	**79.8**	**26.55**

5   Conclusions

The numerical simulations of a thermodiffusion experiment in atmospheric pressure binary mixtures of water and isopropanol subject to micro-vibrations at reduced gravity are presented. It could be concluded that FOTON provides an environment that is conducive to conducting thermodiffusion investigations. In order to understand the behavior of the mixture, the mass fraction of the individual species, the temperature, velocity, the thermodiffusion coefficients and density were studied at different horizontal and vertical lines in the cavity. It was observed that the mole fraction of water began to increase at the location near the hot wall for a mixture with negative Soret effect. Isopropanol experienced a strong separation for FOTON cases; in addition, in the cavity with shorter length, pronounced diffusion occurred. It was found that, for all cases, the separation direction was opposite and weaker for the mixture with 0.5 isopropanol mass fraction as a result of positive Soret effect and unsteady condition. In this low pressure binary mixture, we notice even higher errors for the ISS case; however, these errors are much smaller for FOTON cases but it should be mentioned that all the errors are significant and greater than 25 percent. Thus, this kind of investigation should be considered for experiment on board satellites or space vehicles. The diffusion coefficients, density and viscosity were variable in this investigation, so that the correctness of assumptions was proved by observing the significant difference of these parameters on simulation results.

by the Canadian Space Agency (CSA). The author also acknowledges the support and useful suggestions of his colleagues Mr. Parsa and Dr. Srinivasan at Ryerson University.

References

Bongers, H., & Goey, L. d. (2003). the flat flames study. *Combust. Sci. Technol.*, vol. 175, pp. 1915-1928.

Chacha, M., & Saghir, M. Z. (2005). Solutal-Thermo-Diffusion Convection in a Vibrating Rectangular Cavity. *International Journal of Thermal Sciences*, vol. 44, pp. 1-10.

Duhr, S., & Braun, D. (2011, 1). Why molecules move along a temperature gradient. *Proceedings of the National Academy of Sciences* , pp. 19678-19682,103(53).

Elhajar, B., Mojtabi, A., Catherine, M., & Mojtab, C. (2009). Influence of vertical vibrations on the separation of a binary mixture in a horizontal porous layer heated from below. *International Journal of Heat and Mass Transfer*, vol. 52, pp. 165-172.

Ern, A., & Giovangigli, V. (1998). Thermal diffusion effects in hydrogen/air and methane/air flames. *Combust. Theory Modell*, vol. 2, pp. 349-372.

Grcar, F., Bell, B., & Day, S. (2009). The Soret effect in naturally propagating, premixed, lean, hydrogen–air flames. *Proceedings of the Combustion Institute*, vol. 32, pp. 1173-1180.

Rogers,J.B., Hrovat, M., & McPherson, K. (2002). *Accelerometer data analusis and presentation techniques.* Lewis Research Center, Tal-Cut. Cleveland, Ohio 44135: NASA.

Joachim, G., & Gabriele, S. (2001). Perturbed-Chain SAFT: An Equation of State Based on a Perturbation Theory for Chain Molecules. *Ind. Eng. Chem. Res*, vol. 40, pp. 1244-1260.

Mojtabi, M., Razi, Y., Maliwan, K., & Mojtabi, A. (2004). Influence of vibrations on Soret-driven convection in porous media. *Numerical Heat Transfer Part A: Applications*, vol. 46, pp. 981-993.

Monti R., Savino R., Lappa M. (2001): On the convective disturbances induced by g-jitter on the space station, *Acta Astronautica*, Vol. 48, No. (5-12), pp. 603-615.

Parsa, A., & Saghir, M. (2011). Thermodifussion in a binary fluid mixture subjected to external vibration; effect of variable physics properties. *ASME/JSME*. Honolulu, Hawaii, USA.

Parsa, A., Srinivasan, S., & Saghir, M. Z. (2010). Impact of Density Gradients

on the Fluid Flow Inside a Vibrating Cavity Subjected to Soret Effect. *Physics of Fluids , Submitted*.

Patankar, S. V. (1980). *Numerical Heat Transfer and Fluid Flow.* Minnesota: Taylor and Francis.

Platten, J. (2003). in Proceedings of the 5th International Meeting on **Thermodiffusion** (IMT5). *Philos. Mag.*, vol. 83, pp. 17-18.

Shukla, K., & Firoozabadi, A. (1998). A new model of thermal coefficients in binary hydrocarbon mixtures. *Ind. Engineering. Chemical*, vol. 37, pp. 3331-3342.

Srinivasan, S., & Saghir, M. Z. (2009). Experimental Data on Thermodiffusion in Ternary Hydrocarbon Mixtures. *Journal of Chemical Physics*, vol. 131, p. 124508.

Srinivasan, S., & Ziad Saghir, M. (2010). Experimental Approaches to Study Thermodiffusion. *Elsevier*.

Srinivasan, S., Dejmeck, M., & Saghir, M. Z. (2010). Thermo-Solutal-Diffusion in high pressure Liquid Mixtures In the Presence of Micro-Vibrations. *International Journal of Thermal Science*, vol. 10, no. 49, pp. 1613-1624.

Srinivasan S. and Saghir M. Z. (2011): Impact of the Vibrations on Soret Separation in Binary and Ternary Mixtures, *Fluid Dyn. Mater. Process*, Vol. 7, No. 2, pp. 201-216.

Tai, B.-C., & Char, M.-I. (2010). Soret and Dufour effects on free convection flow of non-Newtonian fluids along a vertical plate embedded in a porous medium with thermal radiation. *International Communications in Heat and Mass Transfer*, vol. 37, pp. 480-483.

Yan, Y., Jules, K., & Saghir, M. Z. (2008). A Comparative Study of G-jitter Effect on Thermal Diffusion Aboard the International Spacestation. *Fluid Dynamics and Material Processing Journal*, vol. 3, no. 3, pp. 231-245.

Zeng-Yuan, G., Zhi-Xin, L., & Xiao-Bing, L. (2002). Size effect on free convection in a square cavity.